Charged-species profiles in electronegative radio-frequency plasmas

D. Vender, W.W. Stoffels, E. Stoffels, G.M.W. Kroesen, and F.J. de Hoog
Department of Physics, Eindhoven University of Technology,
P.O. Box 513, 5600 MB Eindhoven, The Netherlands
(Received 14 September 1994; revised manuscript received 10 November 1994)

The negative ion density profile in a low pressure oxygen rf plasma has been measured by a photodetachment technique. At an rf power of 10 W and a neutral pressure of 10 mTorr, a parabolic negative ion density profile is obtained with a peak density of 8×10^{15} m^{-3} and a maximum ratio of negative ion to electron densities $n_-/n_e \approx 18$. Under these conditions, the most abundant positive ion, determined by ion mass spectrometry, is O_2^+ with O^+ being less than 10% of the positive ion density. The most abundant negative ion is O^- with O_2^- and O_3^- being less than 20% of the total negative charge density. The maximum in the density profile of negative ions shifts closer to the powered rf electrode as the pressure is increased in the asymmetric system. Comparison of the results to theory indicates that the asymmetry follows from an enhancement of the ionization rate near the powered electrode sheath. The parabolic profile is also obtained in CCl_2F_2 at low pressure. Simulations and measurements show a rapid drop in ion density near the sheath that may be related to the recently discussed "stratification" phenomenon in electronegative plasmas.

PACS number(s): 52.80.Pi, 52.25.Fi, 52.40.Hf, 52.50.Dg

I. INTRODUCTION

The influence of negative ions on discharge structure and the sheaths has attracted renewed interest recently [1–6] since many of the gases used in technological applications such as plasma etching readily form stable negative ions. The presence of negative ions in the rf plasmas used in applications can be expected to affect discharge behavior. Negative ions have also been linked to powder formation in chemically active plasmas, a factor which further accentuates their importance [7,8].

In this paper spatially resolved measurements of the negative ion densities in a radio-frequency plasma in oxygen at low pressure are presented and compared to theory. All of the measurements were performed at an rf power of 10 W and pressures between 5 and 150 mTorr. Under these conditions the dissociation degree in the discharge is low and the plasma composition can be expected to be simple, with O_2 the dominant neutral species, O^- the dominant negative ion, and O_2^+ the dominant positive ion. However, the generation and loss mechanisms for the charged species are strongly affected by the pressure and this in turn affects the density profiles. At the lowest pressures, the ion density profiles are parabolic. As the pressure is increased, more complex, asymmetric profiles are observed and it is shown that this asymmetry is mainly due to spatially nonuniform positive ion production. The results obtained in oxygen are compared to measurements in CCl_2F_2 and a mixture of argon and CCl_2F_2.

The experimental details are given in Sec. II. In Sec. III we consider the discharge kinetics and the charged particle balance with the simplifying assumptions which lead to the parabolic density profiles. The results are presented in Sec. IV.

II. EXPERIMENT

The experimental arrangement consists of a capacitively coupled rf plasma confined in an aluminium cylinder with a diameter of 17.5 cm and a height of 5 cm. The experimental apparatus and the method of measuring the electron and negative ion densitites are described in detail in the preceding paper [9]. The gas flow in the present experiments was kept at 30 SCCM (SCCM denotes cubic centimeter per minute at STP) and the pressure was varied between 2.5 and 200 mTorr. The total input power was kept constant at 10 W for oxygen plasmas. Electronegative plasmas were also obtained in CCl_2F_2 and in a mixture of argon and 10% CCl_2F_2 with an input power of 50 W. For the purpose of comparison to simple models and simulations, the experimental conditions were chosen to keep the plasma composition in both O_2 and Ar+CCl_2F_2 plasmas as simple as possible—with one type of negative ion and one type of positive ion carrying most of the charge. A higher input power was used for plasmas generated in CCl_2F_2 and Ar+CCl_2F_2 in order to obtain higher densities and thus improve the signal-to-noise ratio.

As explained in Ref. [9], the aluminium cylinder enclosing the plasma serves as a resonant microwave cavity for the measurement of the total electron density and, in combination with photodetachment, the negative ion density profiles. The cavity is excited in the TM_{020} mode, which has a Bessel function radial dependence with a central field maximum, so the technique is sensitive mainly on the cavity axis. The axial resolution of the method is determined by the beam diameter, which is set by a diaphragm with an aperture diameter of 2 mm. Axial profiles are obtained by displacing the whole plasma chamber with respect to the fixed laser beam. By varying

the laser wavelength (from the fundamental at 1064 nm through to the frequency quadrupled beam at 266 nm) it is possible to separate several types of negative ions. For example, O_2^- with a electron affinity of 0.44 eV can be distinguished from O^- (1.46 eV) and O_3^- (2.10 eV), and Cl^- (3.6 eV) can be distinguished from F^- (3.4 eV).

Several sources of error arise in the density measurements. Although the field averaged electron density can be determined to better than 0.1%, uncertainties in the electron density profile lead to errors of about 10% in the value of the electron density in the plasma glow. In this work we assume that the electron density in the plasma is constant (see Sec. III), that the electron density in the sheaths can be neglected, and that the edge of the glow corresponds to the position where the negative ion density drops to zero. The negative ion density measurement is subject to additional sources of error. The laser beam passes through a diaphragm which helps to define the laser beam volume; however, uncertainty in the beam diameter results in about a 20% error in the negative ion density. We note that this error does not affect the shape of the profiles. Another source of error is due to the radial averaging of the photodetached electron density. We have assumed that the radial profile of the negative ion density does not depend strongly on axial position. This facilitates comparison of the measurements to one-dimensional theory. Ignoring variations in the radial density profiles is not a very serious source of error since the detection method has enhanced sensitivity near the cavity axis, but errors of about 5% which can affect the axial profile shape are expected. Finally, fluctuations in the plasma and other sources of noise in the system necessitate averaging over a number of laser pulses. Each density value represents typically ten laser pulses. Only the latter two sources of error affect the profile shape and the error arising from fluctuations depends on the experimental conditions. A worst case estimate, applying, e.g., at low ion density, is an error of ~30%, but the total relative error in the profiles is typically less than 10%.

III. THEORY

Two issues are considered in order to ascertain the expected density profiles: the plasma composition is determined from the discharge kinetics and the density profiles are then obtained by solving the relevant species continuity equations. A global kinetic model of the oxygen discharge under consideration here has been developed and published in the preceding paper [9]. In the pressure range under consideration, the main negative ion formation mechanism is dissociative attachment while the destruction mechanisms for the negative ions are pressure dependent. Positive ions are created in electron impact ionization and diffusion of the positive ions to the wall where they recombine is the most important loss mechanism for positive ions in oxygen. Mutual neutralization with negative ions has a large rate coefficient, but this process is always less important in the low pressure, low density oxygen plasma. In contrast, wall loss is more important than mutual neutralization only for the lowest pressures (~ 2.5 mTorr) in CCl_2F_2. The ion loss frequencies due to these two mechanisms will be compared for oxygen plasmas after the expected density profiles are derived.

Consideration of the discharge kinetics [9] suggests that the oxygen plasma can be effectively modeled by considering only three charged species: electrons, O^-, and O_2^+. While the densities of O_2^- and O_3^- can be comparable to the electron density, they are of secondary importance for the total negative ion density which we are considering. Electrons of course cannot be ignored since they are responsible for ion generation. In the simplest model of the discharge we therefore consider the continuity equations for the three charged species

$$\nabla \cdot \Gamma_e = (k_{\text{ion}} - k_{\text{at}}) n_e(n_g, n_{O_2(a)}) + k_{\text{det}} n_- n_{O_2(a)} \quad (1)$$

$$\nabla \cdot \Gamma_+ = k_{\text{ion}}(n_g, n_{O_2(a)}) n_e - k_{\text{rec}} n_+ n_-, \quad (2)$$

$$\nabla \cdot \Gamma_- = k_{\text{at}}(n_g, n_{O_2(a)}) n_e - k_{\text{rec}} n_+ n_- - k_{\text{det}} n_- n_{O_2(a)}, \quad (3)$$

where the subscripts on the flux Γ and the density n refer to electrons O_2^+ and O^-, n_g is the ground state and $n_{O_2(a)}$ the metastable neutral gas density, and k_{ion}, k_{at}, k_{rec}, and k_{det} are the rate coefficients for ionization, attachment, recombination (mutual neutralization), and detachment. The fluxes are given by

$$\Gamma_i = -D_i \nabla n_i + q_i n_i \mu_i E \quad (4)$$

with $i = e$, $+$, and $-$, D_i the diffusion coefficients, μ_i the mobilities, E the electric field, and $-q_e = q_+ = -q_- = 1$.

Charge neutrality and current balance

$$n_+ = n_e + n_-, \quad (5)$$

$$\Gamma_+ = \Gamma_e + \Gamma_- \quad (6)$$

complete the system of equations for the three-component plasma. It should be noted that the response of the ions to the rf modulation of the electric field is negligible and the rf modulation of the electron density is only significant in the sheath regions. The electric fields E and the electron density n_e can thus be replaced by time averages in the above equations when only the plasma bulk is under consideration. In the same way we may consider ion production using time averaged rates and ignore any time dependence in the model.

Models of the electronegative plasma similar to the present one have recently been investigated by Franklin *et al.* [11] in connection with positive columns, and for an rf plasma relevant to the present case, by Lichtenberg *et al.* [12]. The ambipolar diffusion coefficients in electronegative plasmas have been given by Thompson [13] and more recently reconsidered by Rogoff [14] and Lichtenberg *et al.* [12]. In the case relevant to our measurements the ambipolar diffusion coefficient for the positive ions D_{a+} can be obtained by eliminating the electric field from the flux equations (4) and assuming Boltzmann equilibrium for both negative species [12,14]. Using the

Einstein relations with μ_-/μ_e, $\mu_+/\mu_e \ll 1$ leads to

$$D_{a+} \approx D_+ \frac{1+\gamma+2\gamma\alpha}{1+\gamma\alpha}, \tag{7}$$

where $\gamma = T_e/T_i$ and $\alpha = n_-/n_e$. Three points are to be noted.

(i) Both the ionization degree and the dissociation degree are low in our low power plasma (typically $< 10^{-4}$ and $< 10^{-2}$, respectively) so the mobilities and the diffusion coefficients in the flux equations (4) can be approximated by the relevant experimentally determined quantities in O_2 gas.

(ii) The assumption of Boltzmann equilibrium for both the negatively charged species is formally incorrect. It is nevertheless a good approximation and is justified *a posteriori* by consideration of the relevant lifetimes and collision frequencies and by checking against simulations.

(iii) The presence of negative ions considerably alters the usual ambipolar diffusion of charged species. Indeed, when the negative ion density is high the electron temperature no longer appears in the positive ion diffusion coefficient. The application of the term "ambipolar diffusion" to electronegative plasmas where the ion fluxes are determined primarily by volume reactions and not by the equality of wall fluxes has been criticized recently [11]. However, it is clear that the motion of the charged species is still affected by the self-consistent field which arises from the necessity of total current balance.

We now consider the positive ion density profile for α large, which is the condition relevant to the measurements at low pressure [9], with the usual temperature ordering for the weakly ionized, low pressure plasma

$$T_e \gg T_+ = T_-. \tag{8}$$

For $\alpha \gg 1$ Eq. (7) becomes

$$D_{a+} \approx 2D_+. \tag{9}$$

At the lowest pressures we may assume that the positive ion profile is determined by ionization and wall loss with recombination being negligible. Furthermore, the Boltzmann relations for the negatively charged species imply

$$\nabla n_e = \frac{\nabla n_-}{\alpha\gamma}, \tag{10}$$

so the electron density gradient in the glow can be neglected, giving a uniform density in the plasma and, at low enough pressure, a uniform ionization rate. We note that the electron density profile remains flat even when the electron temperature varies in the discharge gap as long as $T_e \gg T_+, T_-$. The simplest form of the positive ion continuity equation is now

$$-D_{a+}\frac{d^2 n_+}{dx^2} = k_{\text{ion}} n_g n_{0e} \tag{11}$$

with $n_{e0} = \langle n_e \rangle$. Equation (11) can be integrated to give the parabolic density profile

$$n_+(x) = \frac{k_{ion} n_g n_{e0}}{2D_{a+}}(l^2 - x^2), \tag{12}$$

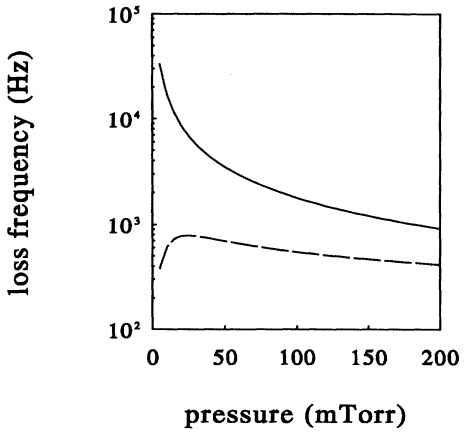

FIG. 1. Positive ion loss frequencies in oxygen due to wall loss (solid line) and recombination (dashed line) at 10 W.

where $2l = H_g$ is the width of the glow region.

The simple parabolic ion density profile has been recently derived by Lichtenberg *et al.* [12] and observed in numerical simulations of electronegative rf plasmas [15,16,12]. It provides a framework in which our assumptions can be evaluated. The loss rate of positive ions to the wall is given by D_{a+}/Λ^2 where the effective loss length $\Lambda = H_g/\sqrt{12}$ [9] with H_g the glow width. A comparison between the loss frequencies of the positive ions due to wall loss and recombination ($k_{\text{rec}} n_-$) is shown in Fig. 1 and it is clear that for low pressure (< 50 mTorr), ignoring the effect of recombination on the positive ion profile is permissible.

Figure 2 shows a comparison of the loss frequencies for the electrons. The wall loss for electrons is equal to the positive ion wall loss by current balance and it is the dominant electron loss mechanism at the lowest pressures (< 10 mTorr). At higher pressure the electron loss is due mainly to dissociative attachment to O_2. Since the electron mean free path for momentum transfer is approximately 6 cm at 10 mTorr [17], reflection

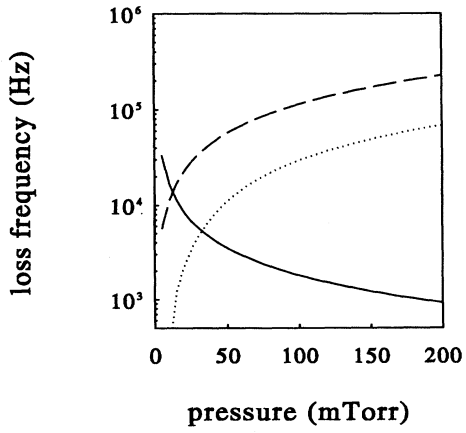

FIG. 2. Electron loss frequencies in oxygen due to wall loss (solid line), attachment to O_2 (dashed line) and attachment to metastable states (dotted line) at 10 W.

of electrons at the sheath is important at low pressure and this increases the effective collision frequency for the electrons. In any case, the collision frequency for the electrons ($\nu_m \approx 1.9 \times 10^9 p$, with pressure p in Torr) is more that three orders of magnitude greater than the total loss frequency for the whole range of pressure investigated, validating the assumption of Boltzmann equilibrium for the electrons.

The loss frequencies for the negative ions are plotted in Fig. 3. Direct ionization is always negligible. At low pressure recombination is dominant whereas detachment in collisions with O_2(a) dominates for $p > 20$ mTorr. This increase in the negative ion loss rate at high pressure is responsible for the decrease in the density above 30 mTorr seen in Fig. 11 of Ref. [9]. Detachment in collisions with O is less important. Since the wall loss of the O_2(a) metastable states is slow (with a sticking coefficient $\approx 10^{-3}$ [10]), the metastable profile is flat and negative ion loss due to collisions with metastable states is uniform. The momentum transfer frequency for the negative ions can be estimated from their mobility using $\mu_- = e/m_r\nu_m$, where m_r is the reduced ionic mass. The mobility of O^- ions in O_2 is $\mu_- = 3.2 \times 10^{-4}$ m^2/V s [18], which gives $\nu_m \approx 3.4 \times 10^7 p$, with the pressure in Torr, justifying the assumption of Boltzmann equilibrium for the negative ions.

The cross section for dissociative attachment in oxygen has a threshold at 4.3 eV and peaks at 6.5 eV [19]. At temperatures close to the threshold, the attachment coefficient is only weakly temperature dependent. This implies that for the values of electron temperature expected in this type of discharge (≈ 3 eV [20]) and for uniform electron density, negative ion formation will be reasonably uniform in the discharge gap even with some spatial variation of the electron temperature. With loss and formation both uniform, detachment in collisions with metastables has no effect on the negative ion profile. Recombination, however, is proportional to n_+n_- and, since negative ion formation is uniform, there is a net flux of negative ions towards the center of the plasma where they recombine. This flux is present at all pressures.

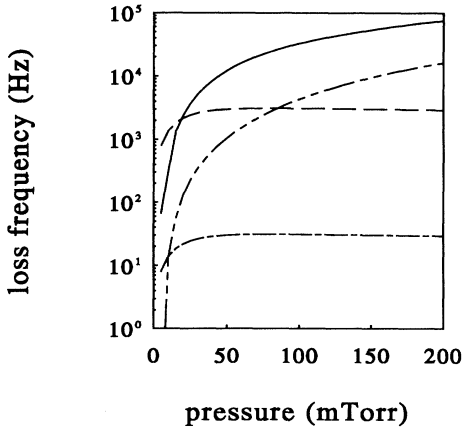

FIG. 3. Negative ion loss frequencies in oxygen due to detachment by O_2(a) (solid line), O (dash–double-dotted line), recombination (dashed line) and ionization (dash-dotted line) at 10 W.

While attachment depends only weakly on T_e, ionization, with a threshold energy of 12.1 eV and a peak cross section at 110 eV [21], depends very strongly on the electron temperature. The ionization rate was assumed to be uniform in the derivation of the parabolic density profile, but it will prove that this is only valid at the lowest pressures where the mean free path for ionizing collisions is sufficiently long. Energetic electrons are expected to be produced mainly in the sheath region in this rf discharge. Both sheath heating and acceleration of secondaries liberated by ion bombardment at the electrodes are expected to contribute to the generation of a suprathermal tail in the electron energy distribution. Furthermore, in our strongly asymmetric discharge, which has an electrode area ratio of about 3, most of the rf voltage appears across the sheath at the (smaller) powered electrode and energetic electron generation will consequently be far more significant at this sheath. The simplest way to model the effect of these electrons on the positive ion density profile is to assume that they are created in the sheath and lost by inelastic collisions as they move into the plasma glow. The ion continuity equation now becomes

$$\frac{d^2n_+}{dx^2} = -\frac{k_{\rm ion}n_g n_{0e}}{D_{a+}} e^{-(x+l)/\lambda}, \tag{13}$$

where λ is an effective loss length for the ionizing electrons and $k_{\rm ion}$ now the ionization rate coefficient at the edge of the powered electrode sheath. Equation (13) can be solved analytically to give profiles of the form

$$n_+(x) = \frac{\lambda^2 k_{\rm ion} n_g n_{e0}}{2D_{a+}} \left(1 + e^{-2l/\lambda} - 2e^{-(x+l)/\lambda} - \frac{x}{l}(1 - e^{-2l/\lambda}) \right). \tag{14}$$

By expanding the exponentials in power series and dropping higher order terms, it can be seen that for $\lambda \gg x$ and l, this expression for the density profiles reduces to Eq. (12). Conversely, when $\lambda \ll x$ and l, the exponential factors can be set to zero and the density goes as $\lambda^2(1 - x/l)$, which corresponds to diffusion away from a planar source.

The effect of recombination on the positive ion density has again been ignored in this treatment. Including recombination and relaxing the assumption that $\alpha \gg 1$ (since this may not be true close to the edge of the glow) gives a more complex equation for positive ion continuity

$$\frac{d}{dx}\left[D_+ \left(2 + \frac{n_{e0}}{(n_+ - n_{e0})} \right] \frac{dn_+}{dx} \right) = -k_{\rm ion} n_g n_{0e} e^{-(x+l)/\lambda} + k_{\rm rec}(n_+^2 - n_+ n_{e0}). \tag{15}$$

This equation is expected to be more applicable at higher pressure, but it does have to be solved numerically for the profile and it is no longer valid near the sheath edge where $n_+ \approx n_e$.

The negative ion profile is derived indirectly by finding first the positive ion profile and using charge neutrality for the negative ion profile $n_-(x) = n_+(x) - n_{e0}$. This approach recognizes the primary role of the positive ions in determining the shape of the profile. Were this approach not applicable, the species continuity equations would have to be solved simultaneously.

IV. RESULTS AND DISCUSSION

The experimentally determined total negative ion profiles are compared to the theoretical profiles in Fig. 4(a) for 10 mTorr Fig. 4(b) for 40 mTorr, and Fig. 4(c) for 100 mTorr. There is very good agreement between the parabolic density profile obtained from Eq. (11) and the experimental data in the low pressure case shown in Fig. 4(a). The two higher pressure cases show considerably more scatter since the data points were averaged over fewer laser pulses during the measurements. The asymmetry due to nonuniform ionization in the discharge gap, discussed in Sec. III, is clearly apparent, especially in the 100 mTorr case. The data have been fitted to profiles obtained from Eq. (14) and there is good agreement between experiment and theory.

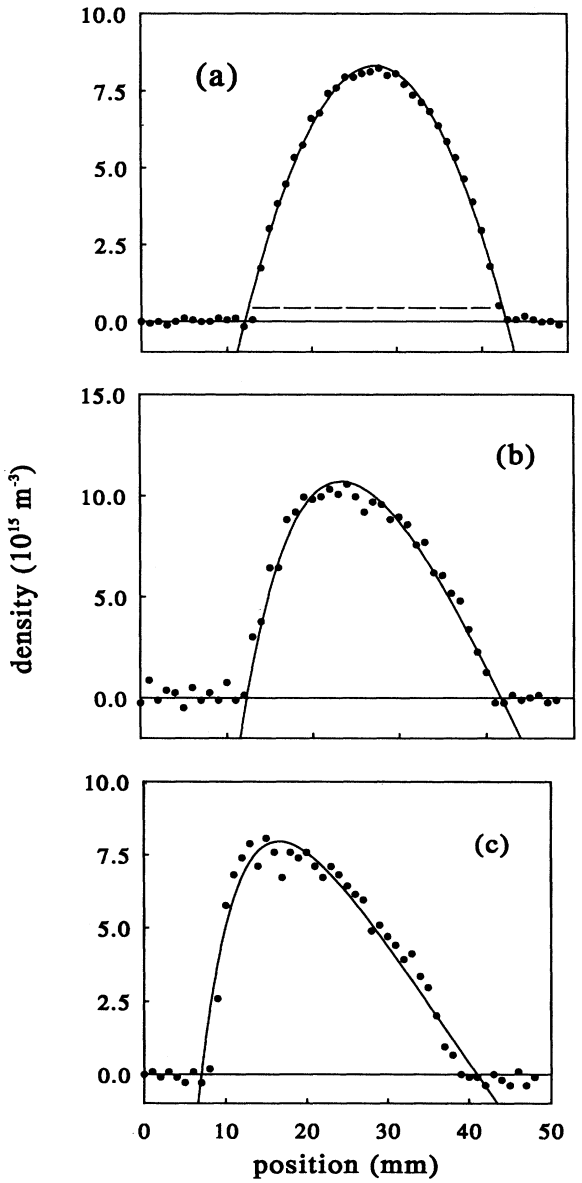

FIG. 4. (a) Negative ion density profile at 10 mTorr oxygen pressure and 10 W input power. The electron density is shown by a dashed line. Data points represent averages over 64 laser pulses. (b) Negative ion density profile at 40 mTorr and 10 W in oxygen. The driven electrode is at the left. (c) Negative ion density profile at 100 mTorr and 10 W in oxygen.

The negative ion density profiles were measured at several values of pressure and each case was fitted by Eq. (14), using charge neutrality to obtain the negative ion profile from the positive ion profile. The effective loss length λ has the expected $1/p$ dependence as shown in Fig. 5. In order to gauge the validity of some of the assumptions leading to the profiles given in Eq. (14), the profiles were also fitted with numerical solutions of Eq. (15), again using charge neutrality for the negative ion profile. Two effects, which are ignored in the derivation of Eq. (14), are included in the numerical solutions: recombination and the spatial variation of the positive ion diffusion coefficient. Comparison between the numerical solutions and the simplified analytic forms shows that recombination has very little effect on the profile shape (even at the higher pressures where it may be expected to be more important) when reasonable values of the recombination coefficient ($< 10^{-12}$ m^3 s^{-1}) are used. The main effect of including recombination is to increase the ionization rate which is necessary to maintain the measured density.

The spatial dependence of the positive ion ambipolar diffusion coefficient is more important than recombination since the positive ion profile is determined primarily by diffusion to the walls. The numerical solutions of Eq. (15) give values of λ which are about 20% higher than those obtained from the analytic fits. Since a longer loss length gives a higher average ionization rate in the discharge gap, the peak ionization rate [k_{ion} in Eq. (15)] must be lowered to compensate. The net result of both

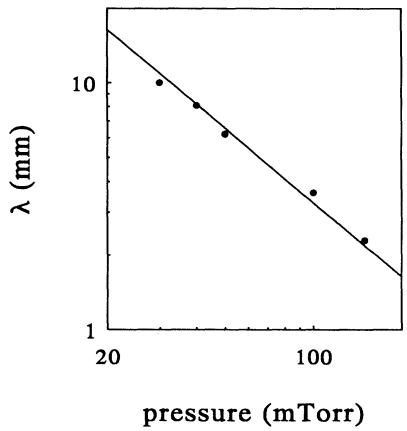

FIG. 5. Effective loss length for ionizing electrons λ as a function of pressure. The line indicates a $1/p$ dependence.

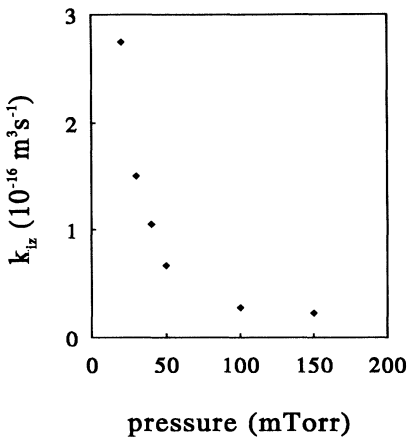

FIG. 6. Ionization rate next to the driven electrode sheath as a function of pressure.

recombination and the change in λ is that the ionization rates from the numerical solutions are not significantly higher at pressures above about 50 mTorr, where the effect of recombination becomes significant. The ionization rate as a function of pressure is shown in Fig. 6, where the values determined from the numerical fits which include recombination are given. Note that ionization is not uniform in the plasma and the peak rates, which occur next to the sheath at the powered electrode, are plotted in the figure. As expected, the ionization rate increases at low pressure, reflecting an increase in the electron temperature. Assuming Maxwellian electron velocity distributions gives values for the electron temperature between 4.1 eV at 20 mTorr and 2.6 eV at 150 mTorr; however, it is unlikely that the electron distribution is Maxwellian at the lowest pressures and the effective temperature of the electrons in the tail of the distribution may be much higher.

The simplified fitting of the density profiles presented above gives good results for the overall profile shape and it is clear that the essential physical processes which determine the profiles are included. But while this approach is attractive, it has important limitations. The first of these is clear from a reexamination of Fig. 4(c), particularly of the data points at positions between 30 and 40 mm. The data values indicate a drop in density next to the grounded electrode sheath which is significantly faster than in the theoretical fit. This phenomenon is apparent at higher pressures in oxygen and it is likely to be due to local ionization near the sheath at the grounded electrode. While the average voltage across this sheath is much smaller than that across the powered electrode sheath, ion energy spectra indicate that the average voltage is still around 60 V, so that secondary electrons from the grounded electrode can easily reach the ionization energy. A more serious limitation is inherent in using only the ion continuity equation for the determination of the profiles since this assumes that negative ion production is uniform; the validity of this becomes questionable as the pressure is increased and electron temperature drops below 3 eV. Under these circumstances the profiles have to be obtained by solving the coupled continuity equations simultaneously.

The parabolic profile shown in Fig. 4(a) is a result of considering only ionization and ion diffusion to the wall with the ionization rate and the diffusion coefficient combining to give one fitting parameter for the profile. Since this effectively ignores gas dependent effects such as the negative ion production and loss mechanisms, the parabolic profile is expected to be universal for three component electronegative plasmas at sufficiently low pressures. In addition to oxygen, parabolic density profiles were measured in CCl_2F_2 and in mixtures of argon with CCl_2F_2. The addition of even small amounts of CCl_2F_2 to argon results in a plasma with almost all of the negative charge carried by negative ions. For example, a 5% partial pressure of CCl_2F_2 in the feed mixture gives an average negative ion density of 4×10^{17} m^{-3} and an average electron density of 2×10^{15} m^{-3}. Ion mass spectrometry of this plasma shows that Ar^+ is the dominant positive ion while selective photodetachment indicates that Cl^- is the most abundant negative ion [22]. These mixtures are thus very useful in comparisons of experimental measurements to models based on very simple treatments of the plasma chemistry [15].

The negative ion profile in a pure CCl_2F_2 plasma is shown in Fig. 7(a) for a total pressure of 2.5 mTorr and an input power of 50 W. The parabolic profile gives a good fit to the data points. In comparison with the oxygen plasma, the plasma generated in CCl_2F_2 has a higher ion density and a higher value of α. These are consequences of the extremely fast attachment rate to CCl_2F_2 and its fragments. The higher density implies that the ion loss by recombination is more than an order of magnitude greater so that recombination can only be neglected at the very lowest pressure (cf. Fig. 1). As may be expected, the profile fitting procedure adopted above for oxygen can also be applied in the case of CCl_2F_2 at low pressure. This is illustrated in Fig. 7(b), where the profile at 5 mTorr is fitted to Eq. (14). The fit to the data is less good than in oxygen and even at 10 mTorr this treatment becomes completely inapplicable and recombination, as well as local ionization at both sheaths, must be included. Figure 7(c) shows the Cl^- density profile at a pressure of 200 mTorr in a mixture of argon and 10% CCl_2F_2. The data have been fitted by a numerical solution of an equation analogous to Eq. (15) but including ionization at the grounded electrode sheath. The rapid falloff of the density away from the powered electrode sheath and the "hollowing out" of the profile are consequences of recombination; these effects can never appear in profiles given by Eq. (14). Similar profiles have been obtained recently in two-dimensional fluid simulations of an asymmetric, electronegative plasma in CF_4 at a pressure of 500 mTorr [23].

As already stated, the analysis of the profile shape presented above is very simple and it is only applicable at low pressure and only within the plasma glow. In particular, it is not applicable in the transition region between the negative ion dominated glow and the sheath which contains essentially only positive ions and

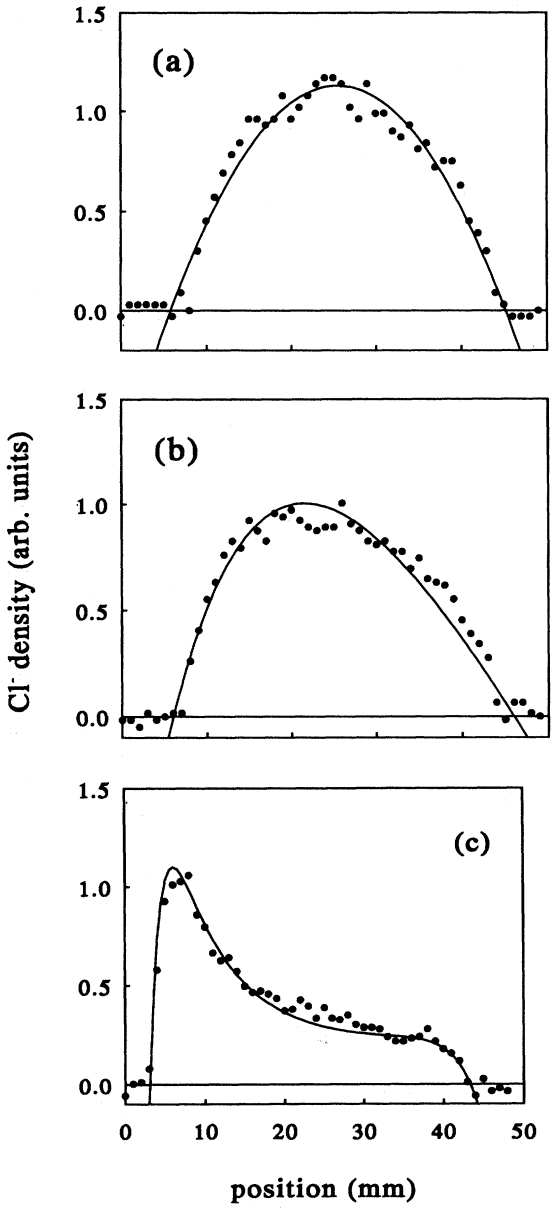

FIG. 7. Density profile of Cl^- ions in CCl_2F_2 at an input power of 50 W at a pressure of (a) 2.5 mTorr and (b) 5 mTorr. (c) Density profile of Cl^- ions at a pressure of 200 mTorr and 50 W power in $Ar+CCl_2F_2$ 10% fitted with a numerically obtained profile.

electrons. The description of this transition region is of great interest since it involves important questions regarding plasma stability, positive ion fluxes to the wall, and the interpretation of probe diagnostics in electronegative plasmas [2]. It has recently been considered theoretically by Tsendin [24], who observes that the plasma may "stratify" spontaneously into two regions with different composition. Calculations by Franklin *et al.* [11] show a similar phenomenon with a very sharp drop in density at the edge of a positive column dominated by negative ions, although the abrupt density drop is present only for unrealistically large values of γ in the calculations [25]. The drop in density near the sheath edge appears to be related to positive ion flux conservation. In the glow where the field is very effectively shielded by the negative ions, the positive ions cannot acquire a substantial drift velocity and their flux to the sheath edge is essentially thermal. In contrast, the ion velocity distribution in the sheath is strongly directed and flux conservation from the glow into the sheath implies a drop in density. The narrow transition region may thus play a similar role to the presheath in electropositive plasmas.

In order to investigate the plasma sheath transition region at the low neutral pressure relevant to our measurements, a hybrid simulation code has been devised which includes a kinetic treatment of the positive ion and electron dynamics and a fluid treatment based on the drift-diffusion approximation for the negative ions. The simulation is one dimensional and electrostatic with sinusoidal voltage applied to one electrode and no external circuit. Positive ion and electron motion is obtained self-consistently using particle-in-cell techniques with Monte Carlo collisions (ionization and elastic scattering for electrons, resonant charge exchange, and elastic scattering for positive ions) [26]. The negative ion density is obtained by solving the continuity equation with an effective field approximation to include the effect of ion inertia [27]. Negative ion processes such as attachment and mutual neutralization have been included, but acceleration techniques are required in order to reach the steady state in tolerable run times. However, at the lowest pressure it is permissible to disregard negative ion generation and loss and thus effectively fix the total number of negative ions at a chosen value, considerably reducing the time needed to reach steady state.

The simulated negative ion profile in a plasma made up of Ar^+, Cl^-, and e^- is compared to a parabola in Fig. 8 for an effective neutral pressure of 20 mTorr and an rf amplitude $V_{rf} = 120$ V. It should be mentioned that the

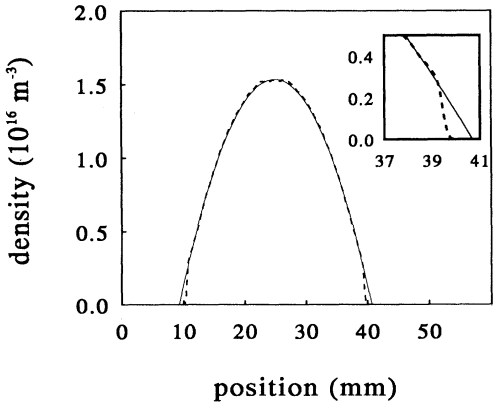

FIG. 8. Simulated density profile of Cl^- ions at a pressure of 20 mTorr with $V_{rf} = 120$ V. The inset shows a detail of the density drop at the glow sheath transition at the grounded electrode. The profile (dashed line) is compared to a parabola (solid line).

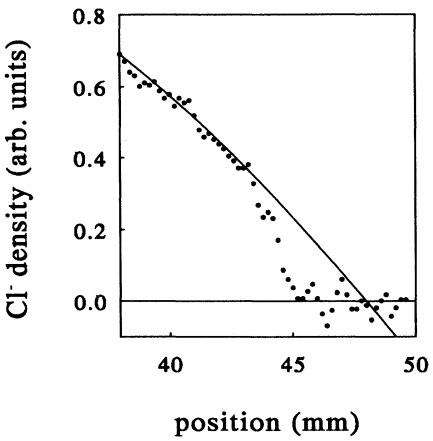

FIG. 9. Density profile of Cl^- ions in CCl_2F_2 near the grounded electrode at 2.5 mTorr and 100 W, measured with a spatial resolution of 0.5 mm. A departure from the fitting by Eq. (14) is evident.

flat electron density profile and the assumption of Boltzmann equilibrium for both negative species prove to be excellent assumptions by checking against the simulation results. The transition region is shown in the inset in Fig. 8. In comparison to the parabolic profile, a relatively rapid drop in density does appear at the sheath edge and it is therefore of great interest to obtain experimental evidence of this phenomenon. However, it is important not to confuse this density dropoff with the effect of local ionization at relatively high pressures [cf. the profile near the grounded electrode in Fig. 4(c)], so we have chosen to investigate low pressures where the ionization profiles are not sharply peaked at the sheaths and CCl_2F_2 where α is larger than in oxygen.

Figure 9 shows the Cl^- density in a pure CCl_2F_2 plasma at 2.5 mTorr and 100 W input power. The spatial resolution was improved to 0.5 mm for these measurements and averages over 64 laser pulses were taken. Equation (14) was used for the fitting since at the higher power the profile becomes slightly asymmetric even at 2.5 mTorr. There is a striking resemblance between the density drop at the sheath edge shown in Fig. 9 and the simulation result, although the two profiles do not correspond to exactly the same conditions. It must be emphasized that the simple profiles fitted to the experimental data and to the simulation results are not expected to apply near the sheath edge; nor will an approach based on Eq. (15) succeed since the increased positive ion diffusion coefficient near the sheath tends to reduce the density gradient. The phenomenon can only be described by an approach that considers all species together, such as the simulation. It can be expected that further experimental investigation of this region together with more realistic simulations will lead to a better understanding of when this phenomenon may occur.

V. CONCLUSION

The average electron density and the axial density profiles of negative ions in an oxygen rf plasma have been measured at low pressure. Comparison of the measurements to a kinetic model indicates that the charged species are predominantly O^- and O_2^+, with electrons making up between 5% and 20% of the total negative charge. Under these conditions the electron density is constant in the plasma glow so the profiles of the charged species can be determined from the negative ion density. The negative ion profile is parabolic at neutral pressures around 10 mTorr, in agreement with theory in which only uniform ionization and diffusion of positive ions to the walls is considered.

At higher pressures the density profile becomes asymmetric and the density peak shifts closer to the smaller electrode in the asymmetric system. Comparison of the cross sections for ionization and dissociative attachment supports the conclusion that the profile asymmetry is mainly a consequence of nonuniform ionization in the discharge gap. The electron temperature derived from the ionization rate next to the driven electrode sheath varies between 4.1 eV at 20 mTorr and 2.6 eV at 150 mTorr, although the electron distribution is unlikely to be Maxwellian at the lowest pressures and effective temperatures in the tail of the distribution may be considerably higher. The parabolic profile obtained at low pressure is independent of the plasma composition and measurements in CCl_2F_2 also show a parabolic profile at 2.5 mTorr.

Simulations and measurements at low pressure indicate that a relatively rapid drop in density can occur at the sheath edge. This may be related to the stratification phenomenon discussed recently in connection with negative ion dominated positive columns.

ACKNOWLEDGMENTS

The authors wish to thank R.K. Porteous, R.N. Franklin, L.D. Tsendin, and I.D. Kaganovich for stimulating discussions. The work of G.H.P.M. Swinkels in helping to run some of the simulations is also acknowledged.

[1] P. Bletzinger, J. Appl. Phys. **67**, 130 (1990).
[2] H. Amemiya, J. Phys. D **23**, 999 (1990).
[3] N.St.J. Braithwaite and J.E. Allen, J. Phys. D Appl. Phys. **21**, 1733 (1988).
[4] H. Shindo and Y. Horiike, Jpn. J. Appl. Phys. **30**, 161 (1991).
[5] R.W. Boswell, A.J. Lichtenberg, and D. Vender, IEEE Trans. Plasma Sci. **20**, 62 (1993).

[6] I.D. Kaganovich, in *Europhysics Conference Abstracts Volume 18E*, edited by M.L.M. van de Sanden (European Physical Society, Eindhoven, The Netherlands, 1994).
[7] A.A. Howling, L. Sansonnens, J.-L. Dorier, and Ch. Hollenstein, J. Appl. Phys. **75**, 1340 (1994).
[8] Contributions to the NATO Advanced Research Workshop on the Formation, Transport and Consequences of Particles in Plasmas [Plasma Sources Sci. Technol. **3** (3) (1994)].
[9] E. Stoffels, W.W. Stoffels, D. Vender, M. Kando, G.M.W. Kroesen, and F.J. de Hoog, preceding paper, Phys. Rev. E **51**, 2425 (1995).
[10] R.L. Sharpless and T.G. Slanger, J. Chem. Phys. **91**, 7947 (1989).
[11] R.N. Franklin, P.G. Daniels, and J. Snell, J. Phys. D **26**, 1638 (1993); R.N. Franklin and J. Snell, *ibid.* **25**, 453 (1992).
[12] A.J. Lichtenberg, V. Vahedi, M.A. Lieberman, and T. Rognlien, J. Appl. Phys. **75**, 2339 (1994).
[13] J.B. Thompson, Proc. Phys. Soc. London **73**, 818 (1959).
[14] G.L. Rogoff, J. Phys. D Appl. Phys. **18**, 1533 (1985).
[15] D. Vender, E. Stoffels, W.W. Stoffels, G.M.W. Kroesen, and F.J. de Hoog, J. Vac. Sci. Technol. A (to be published).
[16] A.J. Lichtenberg, V. Vahedi, and M.A. Lieberman (unpublished).
[17] Assuming a constant momentum transfer cross-section of 5×10^{-16} cm^2, compare G. Csanak, D.C. Cartwright, S.K. Srivastava, and S. Trajmar, in *Electron Molecule Interactions and Their Applications*, edited by L.G. Christophorou (Academic, New York, 1984).
[18] H.W. Ellis, R.Y. Pai, E.W. McDaniel, E.A. Mason, and L.A. Viehland, At. Data Nucl. Data Tables **17**, 177 (1976).
[19] D. Rapp and D.D. Briglia, J. Chem. Phys. **43**, 1480 (1965).
[20] K.F. Al-Assadi, N.M.D. Brown, P.A. Chatterton, and J.A. Rees, Vacuum **42**, 1009 (1991).
[21] T.D. Märk, J. Chem. Phys. **63**, 3731 (1975).
[22] E. Stoffels, W.W. Stoffels, D. Vender, G.M.W. Kroesen, and F.J. de Hoog, J. Vac. Sci. Technol. A (to be published).
[23] J.D.P. Passchier, Ph.D. thesis, Utrecht University, The Netherlands, 1994.
[24] L.D. Tsendin, Zh. Tekh. Fiz. **59**, 21 (1989) [Sov. Phys. Tech. Phys. **34**, 11 (1989)].
[25] R.N. Franklin, in *European Conference Abstracts Vol. 18E* (Ref. [6]).
[26] C.K. Birdsall, IEEE Trans. Plasma Sci. **19**, 65 (1991)
[27] E. Gogolides and H.H. Sawin, J. Appl. Phys. **72**, 3971 (1992).